Solar Energy Materials & Solar Cells 123 (2014) 220–227

Contents lists available at ScienceDirect

Solar Energy Materials & Solar Cells

journal homepage: www.elsevier.com/locate/solmat

Quantification of surface ZnSe in $Cu_2ZnSnSe_4$-based solar cells by analysis of the spectral response

Diego Colombara [a,*], Erika Victoria Christiane Robert [a], Alexandre Crossay [a], Aidan Taylor [b], Mael Guennou [c], Monika Arasimowicz [a], Joao Corujo Branco Malaquias [a], Rabie Djemour [d], Phillip J. Dale [a]

[a] Laboratory for Energy Materials—Université du Luxembourg, 41, rue du Brill, L-4422 Belvaux, Luxembourg
[b] Department of Physics—Durham University, Durham DH1 3LE, United Kingdom
[c] Département Science et Analyse des Matériaux—Centre de Recherche Public Gabriel Lippmann, 41, rue du Brill, L-4422 Belvaux, Luxembourg
[d] Laboratory for Photovoltaics—Université du Luxembourg, 41, rue du Brill, L-4422 Belvaux, Luxembourg

ARTICLE INFO

Article history:
Received 21 June 2013
Received in revised form
17 September 2013
Accepted 4 January 2014

Keywords:
Kesterite
Electrodeposition
ZnSe secondary phase
Short circuit current density
Photocurrent spectroscopy
EQE

ABSTRACT

Absorber layers consisting of $Cu_2ZnSnSe_4$ (CZTSe) and surface ZnSe in variable ratios were prepared by selenization of electroplated Cu/Sn/Zn precursors and completed into full devices with up to 5.6% power conversion efficiency. The loss of short circuit current density for samples with increasing ZnSe content is consistent with an overall reduction of spectral response, pointing to a ZnSe current blocking behavior. A feature in the spectral response centered around 3 eV was identified and attributed to light absorption by ZnSe. A model is proposed to account for additional collection of the carriers generated underneath ZnSe capable of diffusing across to the space charge region. The model satisfactorily reproduces the shape of the spectral response and the estimated ZnSe surface coverage is in good qualitative agreement with analysis of the Raman spectral mapping. The model emphasizes the importance of the ZnSe morphology on the spectral response, and its consequences on the solar cell device performance.

1. Introduction

$Cu_2ZnSn(S,Se)_4$ (CZTS(Se)) is a promising direct band-gap semiconductor for the replacement of $Cu(In,Ga)(S,Se)_2$ from thin film solar cells [1], as demonstrated by devices with power conversion efficiencies above 11% [2]. However, due to the diverse chemistry of Cu, Zn and Sn [3], and to the reduced phase homogeneity region [4], the synthesis of phase-pure CZTS(Se) thin films by chalcogenization of the elemental precursors is a complex task. CZTS(Se) films free from secondary phases are a prerequisite for incorporation into devices. The detrimental effects of Cu–S(Se) [5], Sn–S(Se) [6], Zn–S(Se) [7] and Cu–Sn–S(Se) [8] phases in CZTS(Se)-based solar cells are reported in the literature. Experimentally, it is known that only absorbers with Cu-poor and Zn-rich compositions give rise to devices with reasonable efficiencies [9–13]. From electron beam induced current (EBIC) analysis it was inferred that excess ZnSe on the surface of the absorber in microscopic devices acts as a current blockage [7]. In analogy to the selenide system, this observation was confirmed by an improvement of the short circuit current density (J_{SC}) in CZTS (sulfide) cells where ZnS was selectively removed from the absorber surface by etching with HCl [5]. For the selenide system the harm of Zn excess on the device performance at a macroscopic scale has recently been highlighted to be conditional upon its location [14]. In particular it was shown that segregation of ZnSe at the absorber back contact is neutral on device performance (at least with relatively low minority carrier diffusion lengths), while significant power conversion efficiency reduction is observed when ZnSe is located at the interface between the absorber and CdS, with the J_{SC} reduction accounting for half of the efficiency loss, and the other half being due to deficiency in open circuit voltage and fill factor. If all the photogenerated current under the ZnSe is blocked, then the spectral response of the devices is expected to show a reduction over the entire wavelength range. The loss of response would only depend on the extent of ZnSe coverage at the CZTSe/CdS interface. On the contrary, if any of the current photogenerated under the ZnSe is collected, this should display a characteristic signature in the spectral response of the device. Such a signature would arise from optical absorption of the photons passing through the ZnSe, a phase with optical band gap of about 2.7 eV [15].

In this study a series of sequentially electroplated Cu/Sn/Zn films with Cu poor and Zn rich compositions with respect to CZTSe stoichiometry were selenized and completed into devi

* Corresponding author.
E-mail address: diego.colombara@uni.lu (D. Colombara).

0927-0248/$ - see front matter © 2014 Elsevier B.V. All rights reserved.
http://dx.doi.org/10.1016/j.solmat.2014.01.015

ces. The current–voltage characteristics and spectral response of the devices were measured with the intent of clarifying the effect of surface ZnSe secondary phase on the optoelectronic properties. The spectral response of the devices was modeled in order to account for the wavelength independent collection reduction and for the additional response arising from underneath ZnSe, which is therefore affected by ZnSe optical absorption. The ZnSe surface coverage of the absorber layers determined from the model was compared against values obtained independently from Raman maps.

2. Experimental

The series of CZTSe thin films were obtained by a two-stage route consisting of sequential electrodeposition of Cu/Sn/Zn metal precursors onto 2.5 × 2.5 cm^2 Mo-coated glass substrates, followed by selenization at 550 °C in a graphite box in the presence of Se and SnSe powders, as described elsewhere [11]. The composition of the absorber layers was tuned by varying the relative thickness of the metal layers, so that precursors had either Zn/Sn = 1.2 or 1.3 and Cu/(Zn + Sn) = 0.5, 0.6, 0.7, and 0.8. The electrodeposition was performed in potentiostatic mode with a method adapted from [16]. The setup consisted of a three-electrode cell with a Pt counter electrode, a reference electrode, and a rotating disk working electrode. The potentials employed were −1.07 V (vs. saturated Hg/HgO), −0.75 V (vs. Ag/AgCl) and −1.15 V (vs. Ag/AgCl) for Cu, Sn and Zn respectively. The aqueous electroplating solutions contained 0.1 M $CuSO_4$, 50 mM Sn(II) methanesulfonate and 50 mM $ZnCl_2$ for the depositions of Cu, Sn and Zn respectively.

The composition of the unetched layers after selenization was estimated by top view energy dispersive X-ray spectroscopy (EDS, Oxford Instruments INCA X MAX) with an electron beam of 20 keV. The top view micrographs were obtained with a Hitachi SU-70 scanning electron microscope (SEM), while the layers cross sections were prepared with a focused ion beam microscope (FIB, FEI Helios Nanolab). Pt e-beam deposition was used to prevent damage to the absorber layer during milling and an ion beam with 5 kV acceleration was used to polish the face of the cross section (this also minimizes FIB artifacts, such as material re-deposition [17]). The ion beam was also used to image the absorber cross section using a beam acceleration of 30 kV and a beam current of 9 pA. The ion beam was used for imaging in preference to the electron beam as it provides superior contrast between the various phases while reducing residual topographical information.

Raman maps (40 × 40 μm²) were obtained by means of a Renishaw inVia Micro-Raman spectrometer with an excitation laser wavelength of 442 nm and a power of about 0.5 mW.

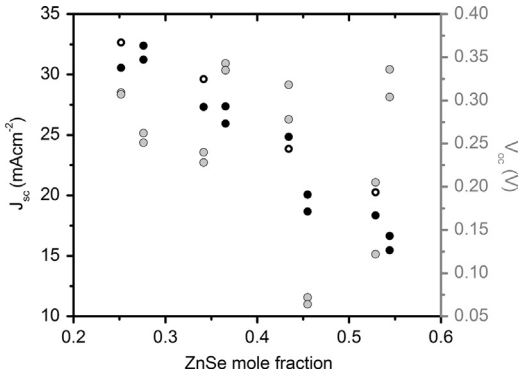

Fig. 1. J_{SC} (black dots) and V_{OC} (grey dots) of the solar cells as a function of the molar ratio of ZnSe in the absorber films calculated from the plating conditions (cf. remark in Section 3.) (the black hollow dots correspond to the devices for which EQE analysis is reported).

Prior to cell finishing, the absorbers were etched in a 5 wt%. KCN solution for 30 s. A CdS buffer layer was deposited by chemical bath deposition, followed by i-ZnO and Al:ZnO depositions by RF-magnetron sputtering. Ni–Al grids were deposited by e-beam evaporation for front contacting. Importantly, the cell finishing procedure of the series of samples was carried out in the same deposition batches, implying that they possess buffer and window layers of the same type and thickness. This is of key importance for the interpretation of the spectral response results.

The room temperature optoelectronic properties of the finished devices were assessed by external quantum efficiency (EQE) and current–voltage (*IV*) measurements using home-built equipment.

3. Results and discussion

The results section is split into three parts. In Section 3.1, the measured optoelectronic properties are described as a function of the amount of ZnSe and the presence of ZnSe on the surface of the absorber layers is confirmed. In Section 3.2, the spectral response is interpreted through the use of a simple model which accounts for both electrical and optical losses. In Section 3.3, some implications of the optical model as a semiquantitative tool are presented.

The microstructural characterizations of the selenized films in this work show that the films are composed solely of CZTSe and ZnSe (cf. Section 3.1). As a consequence, throughout the text the composition of the absorber films is expressed as ZnSe mole fraction defined as the ratio between the moles of ZnSe and the sum of the moles of CZTSe and ZnSe. Due to surface segregation of ZnSe, analysis of the EDS data overestimates the amount of ZnSe in the absorber films (cf. Section 3.1 and Fig. 2a). Therefore, in order to have a more realistic estimation of the ZnSe mole fraction, an approach based on the composition of the precursor films is employed. The Cu and Zn contents of the precursor films are calculated by means of the corresponding electroplating charges and calibrated electroplating efficiencies. The ZnSe mole fraction of the selenized films are then derived assuming no losses of Cu and Zn during the synthesis, with Sn being half the Cu content.

3.1. Experimental results

Regardless of Zn/Sn and Cu/(Zn + Sn) ratios in the precursors, the EDS compositional analysis of the selenized films is consistent with binary mixtures of CZTSe and ZnSe in variable ratios. More precisely, decreasing amounts of Cu in the precursors result in selenized films with increasing ZnSe content. This phenomenon is a direct consequence of the dynamic solid/gas equilibria in the $CZTSe_{(s)}/SnSe_{2(s)}/SnSe_{(g)}$ system [3], and will be discussed more extensively in a separate publication. Fig. 1 shows that a linear relationship exists between the short circuit current density of the devices and the ZnSe mole fraction of the absorber layers (black dots). Other solar cell parameters (e.g. open circuit voltage V_{OC}, grey dots shown in Fig. 1) do not display a clear trend with ZnSe content in the absorber films.

The power conversion efficiencies of the devices range between 0.3% and 5.6%. A linear trend between J_{SC} and composition is also observed if the ZnSe mole fraction in the absorber films is calculated from the EDS analysis; a shift towards higher ZnSe content is observed in such case, indicating that EDS overestimates the amount of ZnSe in the selenized films (data not shown). This observation is related to the depth-dependence of the EDS technique, as confirmed by simulations performed with ThinFilmID Oxford Scientific© software (not shown), and is consistent with the microstructure shown in Fig. 2a, as well as with previous studies [18], i.e. ZnSe segregates mostly on the surface of the films.

The absorber SEM top views (Fig. 2b,c) show the presence of two types of crystals. Films obtained from precursors with high

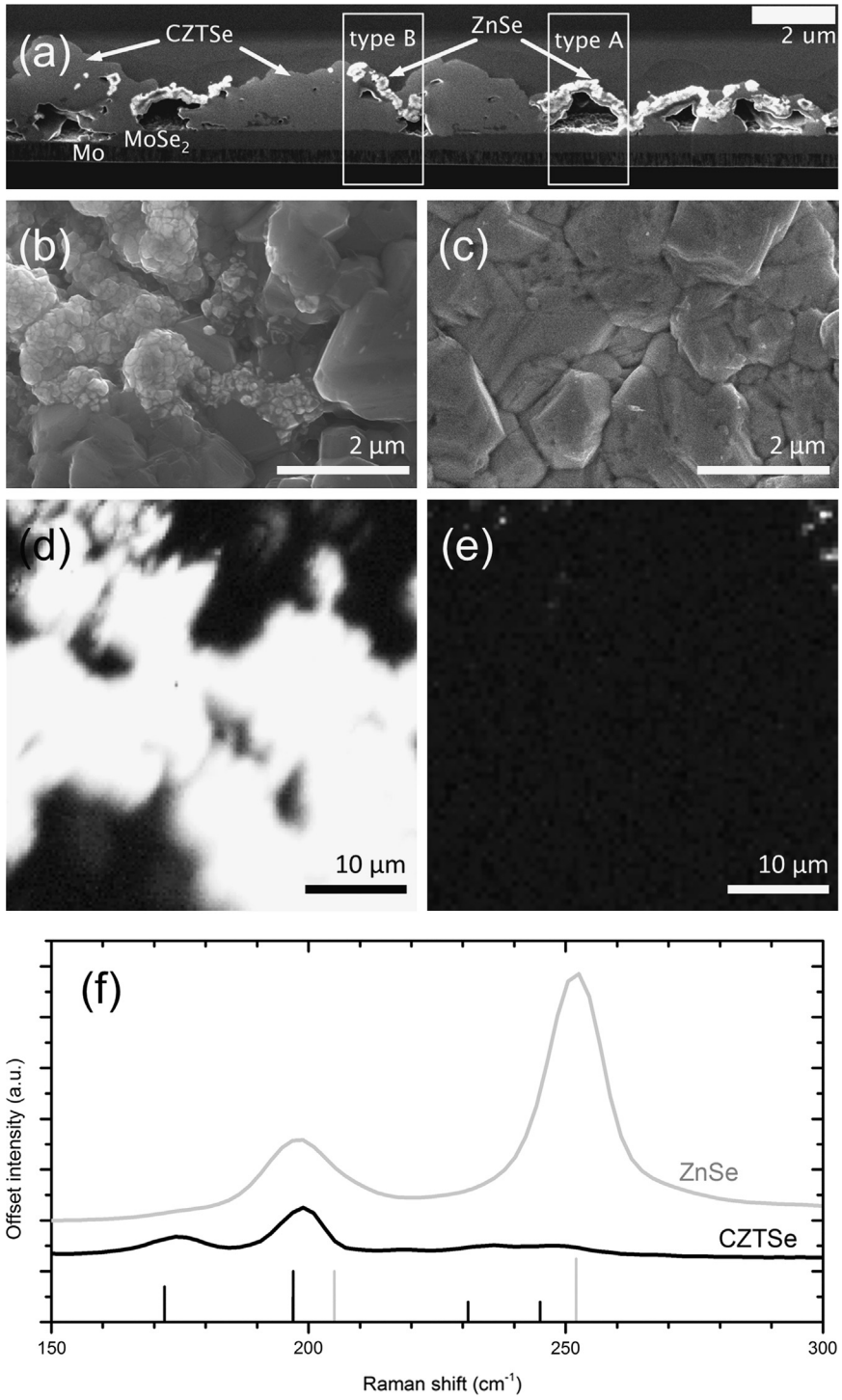

Fig. 2. (a) FIB cross section image of a CZTSe absorber layer with 0.43 ZnSe mole fraction estimated from the precursors plating conditions. FIB/EDS analysis reveals the dark phase to contain Cu, Zn, Sn and Se, while the bright phase contains only Zn and Se, as also observed by Vora et al. [19]. SEM top views (b,c) and Raman maps acquired on different regions (excitation wavelength 442 nm) (d,e) of absorber films respectively with 0.43 (b,d) and 0.25 (c,e) ZnSe mole fractions. (f) Raman spectra obtained from the bright (ZnSe) and dark (CZTSe) areas of the maps with the reference shift positions of CZTSe (black) [20] and ZnSe (grey) [19].

Cu/(Zn+Sn) molar ratio (e.g. Fig. 2c) are mainly composed of micrometer-sized grains. Conversely, Fig. 2b shows that Zn-richer films contain a considerable amount of sub-micrometer-sized crystallites that aggregate on the surface. The SEM top views (Fig. 2b,c) and the Raman maps (Fig. 2d,e), combined with the global EDS analyses suggest that the small crystallites are composed of ZnSe. Both the strongly resonant signal from ZnSe as well as the weaker signature from CZTSe (Fig. 2f) could be unambiguously identified in the Raman spectra from different points of the samples surface, giving rise to highly resolved maps (Fig. 2 d,e). The difference between the measured and the reference Raman shifts of the ZnSe [19] may be attributed to the different structural environment caused by the presence of impurities in the ZnSe, as already inferred by Djemour et al. [18]. The Raman maps were acquired with different focal lengths to ensure results free from artifacts arising from the films roughness, but no meaningful differences were observed. Fig. 2a is the cross section of a film compatible with Fig. 2b,d with 0.43 ZnSe mole fraction. Fig. 2a reveals that the absorber surface alternates between

free CZTSe, large ZnSe aggregates, generally associated with voids in the underlying film (type A in Fig. 2a), and smaller surface ZnSe aggregates in direct contact with CZTSe (type B in Fig. 2a). Assignment of the phases in Fig. 2a is based also on FIB/EDS analysis.

In order to elucidate the dependence of the J_{SC} with the absorber composition and morphology, the external quantum efficiency (EQE) of four solar cells obtained from absorbers with increasing ZnSe content were acquired. The EQEs are shown in Fig. 3.

Fig. 3a shows that an increasing ZnSe fraction in the absorber films results in an overall reduction of the spectral response, as expected. This reduction is approximately independent of wavelength, as highlighted by the similar shapes of the normalized EQEs plotted in Fig. 3b. Normalization suggests that the cause for the variation of J_{SC} is not related to different charge carrier collection lengths, because there is no significant difference between the EQE of the devices in the range 0.9–1.8 eV [23]. Fig. 3b also highlights that in the 2.7–3.2 eV photon energy range the spectra do show a non-generalized spectral variation, indicative of an absorption phenomenon seemingly dependent upon the ZnSe content in the absorber films. Since CdS and Al:ZnO depositions for the series of samples were run in the same batches, absorption variations due to different CdS, ZnO and/or Al:ZnO layers can likely be excluded. On the other hand the location of this spectral feature is consistent with absorption by ZnSe, which has an optical band gap of approximately 2.7 eV [15]. This behavior suggests that some charge carriers generated by photons passing through the ZnSe do get collected.

An explanation for these phenomena must then account for the generalized loss of spectral response and for the limited optical filtering by ZnSe. In order to test these hypotheses, a simplified physical model was created and is outlined in Section 3.2.

3.2. Modeling of spectral response

The physical model that follows was devised to verify the following hypotheses.

1). ZnSe surface segregation is the cause for the overall wavelength independent reduction of spectral response in the CZTSe devices with increasing ZnSe content.

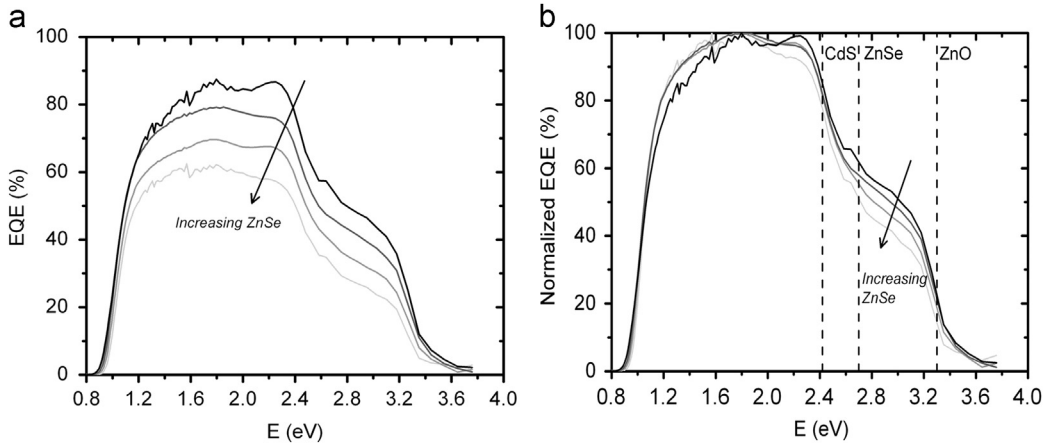

Fig. 3. (a) EQE spectra of devices obtained from absorbers with ZnSe mole fractions of 0.25, 0.34, 0.43 and 0.53. The same spectra are shown in (b) after normalization to the maximum EQE. The band gap values of CdS [21], ZnSe [15], and Al:ZnO [22] are also indicated by the vertical dashed lines.

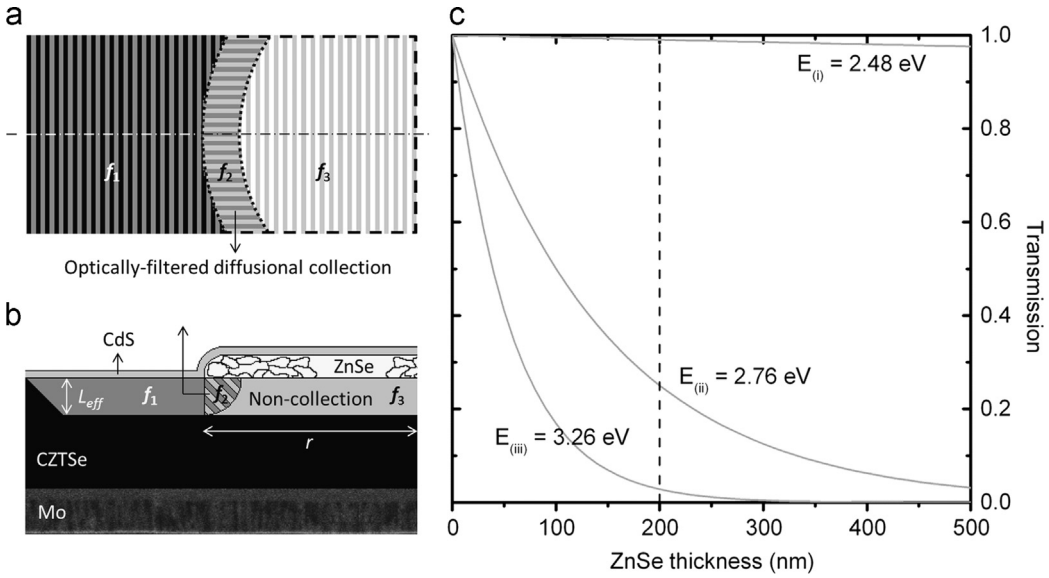

Fig. 4. Top view (a) and cross section (b) 2D schematic models of a Mo/CZTSe/CdS junction with a collection length L_{eff} of 0.2 μm in the presence of a 0.2 μm thick ZnSe surface cluster of radius r 1 μm located at the CZTSe/CdS interface. The volume fractions of absorber layer f_1, f_2 and f_3 are indicated (see text). (c) Attenuation of light intensity as a function of ZnSe thickness for three photon energies: below (i), at (ii) and above (iii) the ZnSe optical bandgap. The dashed line shows the thickness of ZnSe employed in the model.

2). The feature between 2.7 and 3.3 eV in the EQE of the CZTSe devices is a consequence of the optical filtering of the incident photons through the ZnSe clusters.

It is known that the low energy side of the quantum efficiency spectra, near the absorption onset, can be fitted by Eq. (1), derived by Klenk and Schock [24].

$$EQE_\lambda \approx 1-\exp(-\alpha_\lambda L_{eff}) \quad (1)$$

where α is the absorption coefficient of the absorber material and $L_{eff}=w+L_d$ is the effective diffusion length of the minority carriers (aka collection length [25]); with w being the space charge region width and L_d being the minority carrier diffusion length.

Eq. (1) implies that all the radiation absorbed within the collection length generates carriers which are collected. In this work Eq. (1) is assumed to be valid also in the high energy region of the EQE, and is reduced to a step function of value 1 down to the distance within the absorber defined by L_{eff} and zero for distances beyond L_{eff}.

Fig. 4b shows the simplified geometrical model designed to illustrate the physical phenomena involved. It depicts a cross section of the Mo/CZTSe/CdS interfaces, where the CZTSe absorber is partially covered by a circular aggregate of ZnSe crystals. The size of the ZnSe island is defined by its radius r, while space charge region width and minority carrier diffusion length are incorporated into the single parameter L_{eff} for simplicity [24]. This approximation is acceptable if the space charge region width is smaller than the minority carrier diffusion length. Similarly to record efficiency CZTS(Se)-based devices [2], reversed bias EQE measurements of the cells in this work showed negligible improvements in the photocurrent collection. This behavior may be consistent with one of the following possibilities:

(a). High doping density, leading to a small space charge region width
(b). Strong gradient of doping density from the CdS/absorber interface and the edge of the space charge region
(c). Fermi level pinning

Although option (a) seems likely, in any of these cases nothing can be concluded about the relative magnitude of minority carrier diffusion length and space charge region width. The assumption is made that $w < L_d$.

The spectral response of the CZTSe-based devices is modeled by taking into account the following assumptions.

(i). The measured EQE spectrum can be described by a sum of contributions.
(ii). $w < L_d$
(iii). Eq. (1) is valid in the high energy region of the EQE, and is approximated as 1 up to the distance defined by L_{eff} within the absorber and 0 for distances beyond L_{eff}.
(iv). ZnSe blocks any electrical current flow through itself, as inferred by Wätjen et al. [7].
(v). As exemplified in Fig. 4b the volume of potentially active absorber layer is defined only by L_{eff}. This volume of absorber can be divided into three volume fractions, representing different contributions: f_1, f_2 and f_3. f_1 is the volume fraction which surface is free from ZnSe. f_2 is the volume fraction situated underneath ZnSe where photogenerated carriers diffuse and can be collected. f_3 is the volume fraction situated underneath ZnSe where carriers, although generated, cannot be collected. A consequence of this geometrical description is that the sum of f_2 and f_3 (a 3D concept) is numerically equal to the fraction of absorber surface covered by ZnSe, named χ (a 2D concept).
(vi). At high photon energies the internal quantum efficiency (IQE) of the CZTSe is 1 (i.e. the charge carrier generation efficiency is 100%) and the shape of the spectral response is thus limited by buffer and window layers absorption and reflection.

Therefore the starting point of the model is an EQE spectrum of a device without any ZnSe. As a reference ZnSe-free spectral response the model employs the EQE of an 8% efficient CIGSe device [26] with the same buffer and window layers as the CZTSe devices, deposited in consecutive batches. The reference spectrum is obtained by multiplying the original CIGSe EQE by 1.1 to correct for its non-ideal charge carrier generation and is named EQE_R. This choice has the advantage of simplifying the simulation, since absorption and reflection by Al:ZnO, ZnO and CdS are assumed to be equal in the two kinds of devices. Starting from the reference EQE spectrum, the geometrical model considers (Fig. 4a,b) the volume fraction f_1 not covered by ZnSe, and the volume fraction f_2 situated underneath ZnSe that additionally contributes to the spectral response of the devices due to the electron diffusion across to the space charge region located near the CZTSe/CdS interface. Since optical filtering of the incoming light by ZnSe occurs prior to photogeneration of the charge carriers underneath ZnSe, this additional contribution is calculated by taking into account the transmission spectrum of bulk ZnSe, as obtained from the literature [27]. The *Beer-Lambert* law is employed to compute the optical transmission (T_{ZnSe}) of ZnSe with a certain thickness (Fig. 4c) (light reflections due to the additional ZnSe interfaces are neglected).

As a result, the EQE spectrum of the CZTSe device can be expressed by the following:

$$EQE_\lambda = EQE_{R,\lambda}(f_1 + f_2 T_{ZnSe,\lambda}) \quad (2)$$

In Eq. (2) the term f_1 contributes to the spectral response arising from ZnSe free absorber, while the term f_2 takes into account the additional contribution arising from underneath ZnSe.

The interested reader is directed to the Supporting information for details of the 3D mathematical implementation of the geometrical model in Fig. 4a,b, as well as for the dependence of the EQE on the ZnSe surface coverage χ.

Deviations from the reference spectrum EQE_R are implemented by contributions of f_1 and f_2 above, and thus simulated EQE of devices with absorbers containing surface ZnSe were generated (Fig. 5). In order to match the observed film microstructure (Fig. 2a), the modeled ZnSe clusters were chosen to have a thickness of 0.2 μm and a radius r of 1 μm, while L_{eff} was assumed to be 0.2 μm. In Fig. 5(a) the simulated EQE of a CZTSe device with ZnSe surface coverage – χ – varying between 0% and 30% are reproduced in the photon energy range of interest (2.2–4.0 eV).

As expected, addition of ZnSe brings about a generalized reduction of spectral response across the energy range considered in the simulated spectra. Fig. 5(b) shows the simulated EQE spectra normalized to the maximum EQE; this plot highlights the filtering effect due to the collected fraction of charge carriers generated under the ZnSe. Comparison of Figs. 3 and 5 suggests that this simple model allows a satisfactory reproduction of the two main features observed in the measured EQEs.

Given the morphology of the CZTSe absorbers shown in Fig. 2a, one may rightly argue that the model neglects the fact that most of the CZTSe underneath type A ZnSe is actually missing. However, an attentive observation of Fig. 2a reveals that some CZTSe absorber is still present underneath type A ZnSe near the edges. Therefore, the model approximation may be questionable only if L_{eff} was much higher than assumed here (0.2 μm).

With the intent to extract information about the ZnSe surface coverage of the measured devices, the experimental EQE spectra

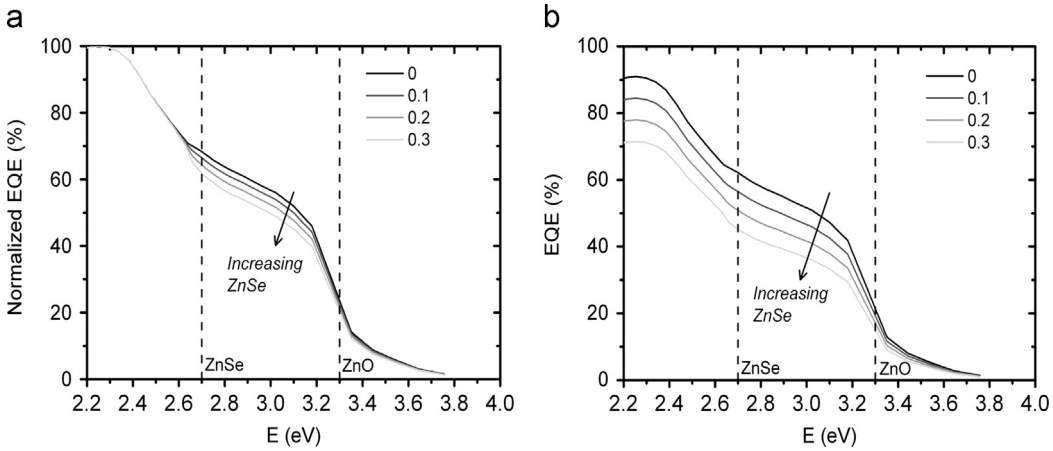

Fig. 5. (a) Simulated EQE spectra with increasing χ from 0 to 0.3. The same simulated spectra are shown in (b) after normalization to the highest value of spectral response. The ZnSe clusters are assumed to be 0.2 μm thick and have a radius r of 1 μm, cf. Fig. 2a; L_{eff} is assumed to be 0.2 μm.

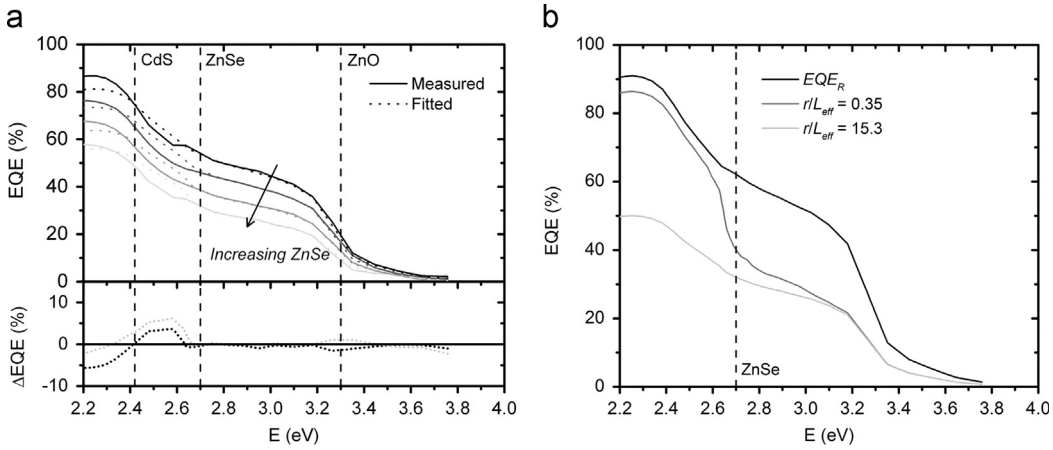

Fig. 6. (a) Overlay of measured EQE spectra of the samples with ZnSe mole fraction of 0.25, 0.34, 0.43, and 0.53 (solid lines) and fitting EQE curves with modeled ZnSe surface coverage χ of 0.15, 0.27, 0.42, and 0.54 (assuming $r=1$ μm, $L_{eff}=0.2$ μm and ZnSe thickness$=0.2$ μm) (dashed lines), and corresponding difference plot (ΔEQE) between fitted and measured EQE for the devices with lowest (black) and highest (light grey) ZnSe mole fraction. (b) Reference spectrum EQE_R and simulated EQEs of CZTSe devices with $\chi=0.5$ (0.2 μm thick ZnSe) with r/L_{eff} of ~0.35 and ~15.3, corresponding to 90% of optical filtering and 90% of current blocking underneath ZnSe, respectively.

shown in Fig. 3 were fitted by means of the thus described model, as to lower the discrepancy between experimental and fitted curves below 2.5% absolute in the photon energy region above the ZnSe optical band gap (2.7 eV). The fitting was performed assuming the same shape of ZnSe clusters for the four samples, changing solely the number of clusters per unit area of absorber, i.e. the ZnSe surface coverage χ. Fig. 6a shows the measured EQE of the samples with ZnSe mole fraction ranging from 0.25 to 0.53 (as shown in Fig. 3a). On the same plot are shown the EQE curves obtained by fitting the measured spectra with the model, by keeping constant r (1 μm), L_{eff} (0.2 μm) and the thickness of the ZnSe clusters (0.2 μm), and varying χ.

The ΔEQE plot in Fig. 6a shows the difference between the fitted EQE curves and the measured EQEs. The features of the experimental EQE spectra are reasonably simulated by the fitting in the photon energy range 2.7–3.8 eV. The fitted EQEs overestimate the spectral response of the samples between the ZnSe and the CdS absorption edges (2.4–2.7 eV). It is possible that this discrepancy arises from ZnSe sub-band gap absorption due to Cu doping [28–32], which is not correctly simulated by the model based on the pure ZnSe absorption spectrum [27]. Another cause could be a slightly different Al:ZnO layer thickness in the ZnSe-free reference sample (displaying different interference fringes), as well as a CdS with slightly different properties, being grown on CZTSe rather than CIGSe.

Besides the ZnSe sub-band gap discrepancy, Fig. 6a clearly shows that the model fails to correctly fit the plateau region of the EQE ($E \leq 2.4$ eV) for the device with lowest ZnSe mole fraction. More precisely, the fitting overestimates the current blocking effect of the ZnSe. Analysis of Eq. (2) and Fig. 4a,b shows that the size of the segregated ZnSe clusters plays a major role in defining the relative volume fractions contributing to the overall spectral response. In this sense, a critical parameter is given by the r/L_{eff} ratio:

If $r / L_{eff} \gtrsim 15.3$ the charge carriers photogenerated under the ZnSe are mostly (> 90%) lost, i.e. the ZnSe acts *de facto* as a current blockage.

If $r / L_{eff} \lesssim 0.35$ collection of the carriers photogenerated under the ZnSe is almost full (> 90%), i.e. the ZnSe acts *de facto* as an optical filter (See the supporting information for the analytical derivation of these two cases).

To clearly highlight the effect of the surface ZnSe morphology on the EQE, simulated EQEs of two samples containing the same total ZnSe surface coverage ($\chi=0.5$) and different r/L_{eff} ratios (15.3 and 0.35) were computed; the plot is shown in Fig. 6b. It is clear from Fig. 6b that ZnSe clusters with finer microstructure allow a

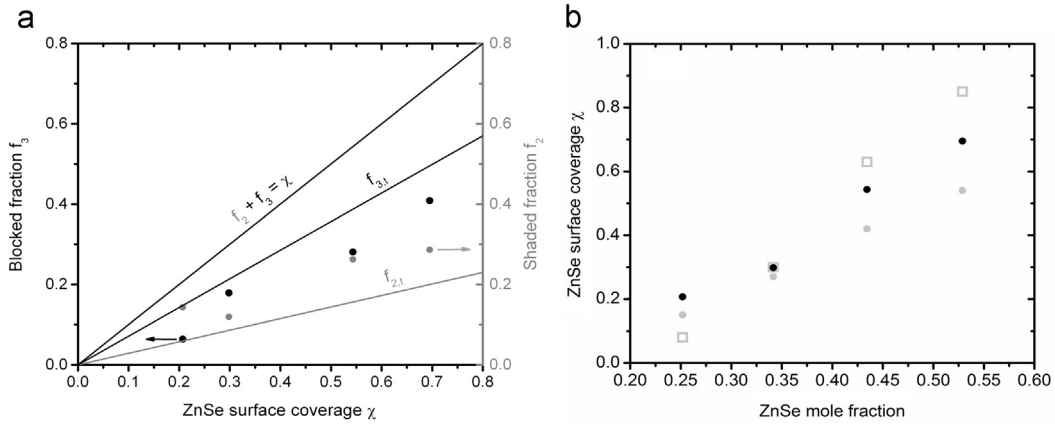

Fig. 7. (a) plot of the volume fractions f_2 (grey) and f_3 (black) of absorber layer subject respectively to charge carrier collection underneath ZnSe and current blocking, as a function of the ZnSe surface coverage χ, according to the geometrically constrained model of Section 3.2 (lines) (assuming $r=1$ μm, $L_{eff}=0.2$ μm and ZnSe thickness$=0.2$ μm) and computed from the measured EQE spectra (circles) for the devices with ZnSe mole fractions of 0.25, 0.34, 0.43, and 0.53. (b) Plot of χ for the same devices in (a) obtained either by fitting of the EQE spectra from Fig. 6a (solid grey), by computation from the EQE spectra using Eq. (2) (solid black) and by pixel counting from the corresponding ZnSe/CZTSe Raman maps (hollow squares).

better collection of charge carriers generated under ZnSe, leading to an increase of spectral response in the plateau region.

3.3. Further semiquantitative implications of the spectral response modeling

The purpose of this section is to illustrate that the surface coverage of ZnSe can also be calculated semiquantitatively considering only a constant ZnSe thickness. The advantage of doing this is that no fitting of the EQE spectrum is required. Finally, ZnSe surface coverages calculated in this section and in Section 3.2 are compared to those obtained independently by Raman spectroscopy.

Further insights can be gained by removing the geometrical constraint imposed by assuming ZnSe clusters of fixed geometrical proportion. This can help understanding the reason for the divergence between the measured EQE spectra and the simulated EQEs for the ZnSe poorest samples in the plateau region ($E \leq 2.4$ eV). Fig. 7a shows the theoretical volume fractions $f_{2,t}$ and $f_{3,t}$ of absorber layer subject respectively to charge carrier collection underneath ZnSe and current blocking, as a function of the ZnSe surface coverage χ for the r and L_{eff} pair chosen in Section 3.2 (1 μm and 0.2 μm, respectively). $f_{2,t}$ and $f_{3,t}$ were derived analytically, and in both cases a linear dependence on χ is obtained (cf. supporting information). The graph is only plotted up to $\chi=0.8$, because for $\chi > \pi/4$ the model implies that the ZnSe islands start to touch, leading to deviation from linearity. The sum of $f_{2,t}$ and $f_{3,t}$ is indicated by the dashed line in Fig. 7a and corresponds numerically to the fraction of absorber's surface area covered by ZnSe, χ.

In addition to the lines $f_{2,t}$ and $f_{3,t}$, the fractions f_2 and f_3 can also be computed from the experimental EQEs, assuming only a fixed thickness of ZnSe. These are also shown as scattered points. Taking into account Eq. (2), f_3 and f_2 were computed from the measured EQEs by looking respectively at the loss of response in the plateau region and at the relative loss in the region of ZnSe optical absorption. Only a ZnSe thickness of 0.2 μm is assumed, while no geometrical relation between f_2 and f_3 is imposed. The reader is referred to the Supporting information for the detailed procedure required to extract f_2 and f_3 from the measured EQEs.

Fig. 7a shows that if the volume fractions of absorber layer subject to current blocking (f_3) and optically-filtered diffusional collection (f_2) are calculated as discussed above, the ZnSe poorest sample displays $f_2 > f_3$. Vice versa, samples with higher ZnSe content have $f_3 > f_2$. The theoretical lines $f_{2,t}$ and $f_{3,t}$ in Fig. 7a were obtained assuming no size variation of the ZnSe clusters as the ZnSe content (i.e. ZnSe surface coverage) in the samples increases. The EQEs fitted with fixed r and L_{eff} values lead to an overestimation of the blocking behavior and to an underestimation of the "optical filtering" effect for the ZnSe-poorest sample. The mismatch between the volume fraction lines and the scattered dots in Fig. 7a signifies that the single pair of r and L_{eff} values employed for the fitting is not suitable to simulate satisfactorily the ZnSe surface coverage for all ZnSe contents. The morphology of the surface ZnSe phase changes considerably with the increase of its mole fraction within the films (Fig. SI6). Therefore, using constant r and L_{eff} for the EQE fitting is a too coarse assumption. As simulated in Fig. 6b, small ZnSe aggregates contribute more to the "optical filtering" effect, while bigger aggregates have a stronger impact on the current blocking behavior.

Fig. 7b shows the ZnSe surface coverage χ extracted with three methods for samples with increasing ZnSe mole fraction. For the black dots χ is estimated from the fitted EQE spectra obtained assuming constant ZnSe clusters size and L_{eff} (Fig. 6a). The solid grey dots are obtained by summing f_2 and f_3 extracted from the experimental EQE spectra by means of Eq. (2). The hollow grey squares are obtained by pixel counting of the ZnSe/CZTSe Raman maps of the corresponding films. In all three cases a linear dependence is found, indicating that the model provides a good qualitative description of the effects of ZnSe surface coverage on the spectral response of CZTSe-based solar cell devices. The disagreement in absolute values stems from the fact that Raman mapping does not average large enough areas of the films.

4. Conclusions

This work shows that some charge carriers generated underneath surface ZnSe can be collected. The presence of ZnSe on the surface of CZTSe absorber layers can be detected by spectral response analysis of the corresponding devices. A simple physical model was formulated to fit the EQE spectra and estimate the ZnSe surface coverage in samples containing variable ZnSe mole fraction. A good qualitative agreement was found between the ZnSe surface coverage estimated from the model and assessed independently by Raman maps analysis. The model can be further implemented if the space-charge region width and the minority carrier diffusion length are known. Likewise, insights into the transport properties of the absorber layer may be gained should the ZnSe morphology be engineered or well known. Indeed, the morphology of the surface ZnSe plays a major role in defining the shape of the device spectral response. For absorber films with

the same extent of ZnSe surface coverage and same collection length it is predicted that devices containing reasonably small ZnSe clusters display higher J_{SC} compared to analogous devices where the clusters have larger size.

The methodology described in this work allows to analyze macroscopically the surface ZnSe content of $Cu_2ZnSnSe_4$-based devices without the specialist need of photoluminescence or blue laser line Raman equipment. Due to the presence of voids in the absorber films underneath large ZnSe clusters, the present work cannot prove that the short circuit current losses are due to surface ZnSe acting as a current blocking phase, although EBIC measurements strongly suggest it is the case [7]. The synthesis and subsequent characterization of a compact CZTSe film with deliberate dispersion of ZnSe islands may provide the ultimate confirmation of the ZnSe current blocking behavior.

Zn-rich and Cu-poor conditions are generally employed to grow good quality CZTSe absorber layers. The future synthetic challenge for the two-stage route will be to minimize the extent of ZnSe segregation, ensuring that the films are free from Cu_2SnSe_3.

Acknowledgments

The authors would like to thank Maxime Thevenin (Université du Luxembourg) and Michael Kirsch (Helmholtz Zentrum Berlin) for device finishing and the CRP Lippmann (Luxembourg) for access to the SEM. We wish to express our gratitude also to Prof. Susanne Siebentritt and to the reviewers of this work for the constructive discussion. The EU seventh framework programme FP7/2007-2013 is acknowledged for funding through the Grant no. 284486.

Appendix A. Supporting information

Supplementary data associated with this article can be found in the online version at http://dx.doi.org/10.1016/j.solmat.2014.01.015.

References

[1] L.M. Peter, Towards sustainable photovoltaics: the search for new materials, Philos. Trans. R. Soc. A: Math. Phys. Eng. Sci. 369 (2011) 1840–1856.
[2] T.K. Todorov, J. Tang, S. Bag, O. Gunawan, T. Gokmen, Y. Zhu, D.B. Mitzi, Beyond 11% efficiency: characteristics of state-of-the-art $Cu_2ZnSn(S,Se)_4$ solar cells, Adv. Energy Mater. 3 (2013) 34–38.
[3] J.J. Scragg, P.J. Dale, D. Colombara, L.M. Peter, Thermodynamic aspects of the synthesis of thin-film materials for solar cells, ChemPhysChem 13 (2012) 3035–3046.
[4] I.D. Olekseyuk, I.V. Dudchak, L.V. Piskach, Phase equilibria in the Cu_2S–ZnS–SnS_2 system, J. Alloys Compd. 368 (2004) 135–143.
[5] A. Fairbrother, E. García-Hemme, V. Izquierdo-Roca, X. Fontané, F.A. Pulgarín-Agudelo, O. Vigil-Galán, A. Pérez-Rodríguez, E. Saucedo, Development of a selective chemical etch to improve the conversion efficiency of Zn-Rich Cu_2ZnSnS_4 solar cells, J. Am. Chem. Soc. 134 (2012) 8018–8021.
[6] B.G. Mendis, M.C.J. Goodman, J.D. Major, A.A. Taylor, K. Durose, D.P. Halliday, The role of secondary phase precipitation on grain boundary electrical activity in Cu_2ZnSnS_4 (CZTS) photovoltaic absorber layer material, J. Appl. Phys. 112 (2012) 173510-1–124508-10.
[7] J.T. Wätjen, J. Engman, M. Edoff, C. Platzer-Bjorkman, Direct evidence of current blocking by ZnSe in $Cu_2ZnSnSe_4$ solar cells, Appl. Phys. Lett. 100 (2012) 173510-1–173510-3.
[8] S. Siebentritt, S. Schorr, Kesterites – a challenging material for solar cells, Progress Photovolt.: Res. Appl. 20 (2012) 512–519.
[9] L. Guo, Y. Zhu, O. Gunawan, T. Gokmen, V.R. Deline, S. Ahmed, L.T. Romankiw, H. Deligianni, Electrodeposited $Cu_2ZnSnSe_4$ Thin Film Solar Cell with 7% Power Conversion Efficiency, Progress in Photovoltaics: Research and Applications, 22 (2014) 58–68.
[10] S. Ahmed, K.B. Reuter, O. Gunawan, L. Guo, L.T. Romankiw, H. Deligianni, A. High, Efficiency electrodeposited Cu_2ZnSnS_4 solar cell, Adv. Energy Mater. 2 (2011) 253–259.
[11] A. Redinger, D.M. Berg, P.J. Dale, S. Siebentritt, The consequences of kesterite equilibria for efficient solar cells, J. Am. Chem. Soc. 133 (2011) 3320–3323.
[12] T.K. Todorov, K.B. Reuter, D.B. Mitzi, High-efficiency solar cell with earth-abundant liquid-processed absorber, Adv. Mater. 22 (2010) E156–E159.
[13] D.A.R. Barkhouse, O. Gunawan, T. Gokmen, T.K. Todorov, D.B. Mitzi, Device characteristics of a 10.1% hydrazine-processed $Cu_2ZnSn(Se,S)_4$ solar cell, Progress Photovolt.: Res. Appl. 20 (2012) 6–11.
[14] W.-C. Hsu, I. Repins, C. Beall, C. DeHart, G. Teeter, B. To, Y. Yang, R. Noufi, The effect of Zn excess on kesterite solar cells, Solar Energy Mater. Solar Cells 113 (2013) 160–164.
[15] S. Venkatachalam, S. Agilan, D. Mangalaraj, S.K. Narayandass, Optoelectronic properties of ZnSe thin films, Mater. Sci. Semicond. Process. 10 (2007) 128–132.
[16] J.J. Scragg, D.M. Berg, P.J. Dale, A 3.2% efficient Kesterite device from electrodeposited stacked elemental layers, J. Electroanal. Chem. 646 (2010) 52–59.
[17] J.T. Wätjen, J.J. Scragg, M. Edoff, S. Rubino, C. Platzer-Bjorkman, Cu out-diffusion in kesterites – A transmission electron microscopy specimen preparation artifact, Appl. Phys. Lett. 102 (2013) 051902-1–051902-4.
[18] R. Djemour, M. Mousel, A. Redinger, L. Gütay, A. Crossay, D. Colombara, P. Dale, S. Siebentritt, Detecting ZnSe secondary phase in $Cu_2ZnSnSe_4$ by room temperature photoluminescence, Appl. Phys. Lett. 102 (2013) 222108.
[19] N. Vora, J. Blackburn, I. Repins, C. Beall, B. To, J. Pankow, G. Teeter, M. Young, R. Noufi, Phase identification and control of thin films deposited by co-evaporation of elemental Cu, Zn, Sn, and Se, J. Vac. Sci. Technol. A: Vac. Surf. Films 30 (2012) 051201-1–051201-7.
[20] M. Grossberg, J. Krustok, J. Raudoja, K. Timmo, M. Altosaar, T. Raadik, Photoluminescence and Raman study of $Cu_2ZnSn(Se_xS_{1-x})_4$ monograins for photovoltaic applications, Thin Solid Films 517 (2011) 2489–2492.
[21] A.E. Rakhshani, B. Pradeep, H.A. Ramazaniyan, The effect of $CdCl_2$ annealing on optoelectronic properties of CSD-grown CdS films, in: D. Lincot, G. Hodes (Eds.), Chemical Solution Deposition of Semiconducting and Non-Metallic Films, Electrochemical Society, New Jersey, USA, 2006, pp. 49–53.
[22] Ü. Özgür, Y.I. Alivov, C. Liu, A. Teke, M.A. Reshchikov, S. Dogan, V. Avrutin, S.-J. Cho, H. Morkoc, A comprehensive review of ZnO materials and devices, J. Appl. Phys. 98 (2005) 041301-1–041301-103.
[23] W.W. Gärtner, Depletion-layer photoeffects in semiconductors, Phys. Rev. 116 (1959) 84–87.
[24] R. Klenk, H.W. Schock, W.H. Bloss, Photocurrent collection in thin film solar cells – calculation and characterization for $CuGaSe_2/(Zn,Cd)_S$, in: Proceedings of the 12th Euoropean Photovoltaic Solar Energy Conference, 1994, pp. 1588–1591.
[25] S. Siebentritt, What limits the efficiency of chalcopyrite solar cells? Solar Energy Mater. Solar Cells 95 (2011) 1471–1476.
[26] J.C. Malaquias, D. Regesch, P.J. Dale, M. Steichen, Simultaneous electrodeposition of indium and gallium from a choline chloride based deep eutectic solvent for Cu(In,Ga)Se2 solar cells, Phys. Chem. Chem. Phys. 16 (2014) 2561–2567.
[27] S. Adachi, T. Taguchi, Optical properties of ZnSe, Phys. Rev. B 43 (1991) 9569–9577.
[28] T. Schwarz, O. Cojocaru-Miredin, P. Choi, M. Mousel, A. Redinger, S. Siebentritt, D. Raabe, Atom probe study of $Cu_2ZnSnSe_4$ thin-films prepared by co-evaporation and post-deposition annealing, Appl. Phys. Lett. 102 (2013) 042101-1–042101-4.
[29] N.K. Morozova, I.A. Karetnikov, V.V. Blinov, E.M. Gavrishchuk, Studies of the infrared luminescence of ZnSe doped with copper and oxygen, Semiconductors 35 (2001) 512–515.
[30] N.K. Morozova, I.A. Karetnikov, V.V. Blinov, E.M. Gavrishchuk, A study of luminescence centers related to copper and oxygen in ZnSe, Semiconductors 35 (2001) 24–32.
[31] G.B. Stringfellow, R.H. Bube, Photoelectronic properties of ZnSe crystals, Phys. Rev. 171 (1968) 903–915.
[32] M. Orita, T. Narushima, H. Yanagita, Transparent conductive Cu-doped ZnSe film deposited at room temperature using compound sources followed by laser annealing, Jpn. J. Appl. Phys. 46 (2007) L976–L978.